Reactive halogen radicals in saline water promote photochemically-assisted formation of manganese oxide nanosheets

Zhenwei Gao, Charlie Skurie, and Young-Shin Jun*

Department of Energy, Environmental and Chemical Engineering, Washington University in St. Louis, St. Louis, Missouri 63130, United States

Address: One Brookings Drive, Campus Box 1180

E-mail: ysjun@seas.wustl.edu

Phone: (314) 935-4539

Fax: (314) 696-1223

http://encl.engineering.wustl.edu/

Environmental Science: Nano

Submitted: April 2022

Revised: July 2022

* To whom correspondence should be addressed

Abstract

Halide ions are naturally abundant in oceans and estuaries. Large amounts of highly saline efflux are also generated and discharged to surface water from desalination processes and from unconventional oil and gas recovery. These highly concentrated halides can generate reactive halogen radicals. However, the redox reactions of halogen radicals with heavy metals or transition metals have received little attention. Here, we report an undiscovered fast oxidation of manganese ions (Mn^{2+}) by reactive halogen radicals. Hydroxyl radicals ($^{\bullet}OH$) are produced by nitrate photolysis. While $^{\bullet}OH$ play a limited role in the direct oxidation of Mn^{2+}, they can react with halide ions to generate reactive halogen radicals to oxidize Mn^{2+}. More Mn^{2+} was oxidized by bromide (Br) radicals generated from 1 mM Br^- than by chloride (Cl) radicals generated from 500 mM Cl^-. In the presence of Br radicals, the abiotic oxidation rate of Mn^{2+} to $Mn(IV)O_2$ nanosheets is greatly promoted, showing a 62% increase in Mn^{2+}(aq) oxidation within 6 hr of reaction. This study advances our understanding of natural Mn^{2+} oxidation processes and highlights unexpected impacts of reactive halogen radicals on redox activities with heavy metals and corresponding nanoscale solid mineral formation in brine. This work suggests a new, environmentally-friendly, and facile pathway for synthesizing MnO_2 nanosheets.

1. Introduction

Interdependent energy-water engineering systems inherently produce large volumes of briny water. To meet rapidly growing clean water demands, desalination processes are increasingly used, consistently generating highly concentrated brine efflux (1.5–2 times as salty as seawater) that are directly released into adjacent lakes, rivers, and near shore seawater.[1, 2] In unconventional oil and gas recovery through hydraulic fracturing, large amounts of concentrated flowback brine (0.9–4.17 M Cl^-, and 9–20 mM Br^-) can accumulate in the surface impoundment before further treatment.[3] As examples, Marcellus and Fayetteville hydraulic fracturing flowback fluids contain about 160 g/L (4.5 M) of Cl^- and 1.8 g/L (22.5 mM) of Br^-.[4] The contaminated surface water from the effluent disposal sites in Pennsylvania contain about 60 g/L (1.7 M) of Cl^- and 40 mg/L (0.5 mM) of Br^-.[4] These highly concentrated halides can be oxidized by the hydroxyl radicals ($^{\bullet}OH$) and triplet state dissolved organic matter to form abundant reactive halogen radicals (e.g., $X^{\bullet}$, $X_2^{\bullet-}$, $XY^{\bullet-}$, where X, Y= Cl, Br, or I).[5] In seawater, which usually contains about 0.54 M Cl^- and 0.8 mM Br^-, the concentrations of their corresponding halogen radicals, e.g., $Br_2^{\bullet-}$ and $ClBr^{\bullet-}$, can be 3–4 orders of magnitude higher than that of $^{\bullet}OH$.[5, 6]

Studies thus far have focused on the effects of reactive halogen radicals on the degradation and transformation of organic pollutants, such as microcystins in estuarine water,[7] and various pharmaceuticals and personal care products (PPCPs) in water treatment processes[8]. In particular, compared to fresh water, seawater increased the photodegradation kinetics of domoic acid (a cis−trans diene) because the generated reactive halogen radicals selectively targeted dienes.[6] In addition, reactive halogen radicals can participate in natural oxidative reactions of mercury (Hg) in the atmosphere. A study conducted in Alaska reported that atmospheric elemental Hg was rapidly converted to reactive gaseous oxidized Hg species by reactive halogen radicals.[9] However,

the roles of reactive halogen radicals in inorganic aqueous systems, such as redox reactions with heavy metal and transition metal ions, remain largely unknown.

Manganese (Mn) oxidation by reactive halogen radicals under the environmental relevant conditions and the roles of reactive halogen radicals in the formation of Mn oxide minerals have never been reported. Mn oxide solids are excellent scavengers of redox-active species and heavy metals in nature, and they play significant roles in geochemical element redox cycling, carbon mineralization, and biological metabolisms.[10-12] In nature, Mn oxide solids are known to be formed by oxidation of Mn^{2+}(aq). In such processes, hitherto, $O_2^{\bullet-}$ has been considered as the most effective radical accomplishing Mn oxidation in both biotic and abiotic systems.[13-17] However, Mn oxidation by reactive halogen radicals in nature has not been considered fully. Laurence et. al (1973) suggested that $Br_2^{\bullet-}$ and $Cl_2^{\bullet-}$, generated by short duration (< 0.1 second) flash photolysis of trihalide ions, oxidized Mn^{2+}(aq) at an extremely low pH (~1), and Mn^{3+}(aq) was proposed to form rather than Mn(IV) oxide solids.[18] Nevertheless, Mn^{3+}(aq) is not stable at circumneutral pH in the absence of a ligand,[19] so it is unclear whether these reactions can occur under environmentally relevant pH conditions. Further, it is unknown whether reactive halogen radicals can facilitate the oxidation of Mn^{2+}(aq) and form nanoscale Mn(IV) oxide solids as the final products for a longer light illumination time rather than within one second.

Here, we show previously unknown effects of reactive halogen radicals on the oxidation of Mn^{2+}(aq) and the fast kinetics of nanoscale Mn(IV) oxide solids formation. Reactive oxygen species (ROS), including $O_2^{\bullet-}$ and $^{\bullet}OH$, were produced during the photolysis of solution containing nitrate.[20] When halides were present in the solution, reactive halogen radicals can be generated by reactions between the halides and $^{\bullet}OH$, increasing the oxidation rate of Mn^{2+} and also increasing the rate and extent of Mn oxide nanosheets formation, compared with the rates of phenomena in

the absence of halides. More Mn^{2+} was oxidized by Br radicals ($Br^{\bullet}$ and $Br_2^{\bullet-}$) generated from 1 mM NaBr than by Cl radicals ($Cl^{\bullet}$ and $Cl_2^{\bullet-}$) generated from 500 mM NaCl. In addition, δ-MnO_2 nanosheets were formed by reactive halogen species. The crystallinity of the formed Mn oxide nanosheets was affected by the ionic strength. This newly discovered reaction mechanism between Mn^{2+}(aq) and reactive halogen radicals under environmental relevant conditions can advance our understanding of nanoscale Mn oxide solids formation in the environment, and can help to predict its redox activities, such as scavenging and oxidation of heavy metals (As, Pb, and Cr) and geochemical elements (S, N, and P).

2. Materials and methods

2.1 Chemicals and materials

All chemicals used in this study were at least American Chemical Society grade. Manganese chloride ($MnCl_2$, 97%, anhydrous) was purchased from Beantown Chemical Co. (NH, USA). Crystal sodium nitrate ($NaNO_3$, ≥ 99.0%) was obtained from Avantor Performance Materials, Inc. (PA, USA). Leucoberbelin blue I (LBB, 65%), potassium permanganate ($KMnO_4$, > 99%), sodium sulfate (Na_2SO_4, ≥ 99%), Sodium bromide (NaBr, ≥ 99.99%), superoxide dismutase bovine (SOD, > 90%), and 2-bromoacetophenone (BrAP, > 98%) were purchased from Sigma-Aldrich. Sodium hydroxide (NaOH, > 97%) and sodium chloride (NaCl, > 99%) were bought from VWR International LLC. Deionized (DI) water (resistivity ≥18.2 MΩ·cm, Barnstead Ultrapure water systems) was used to prepare the solutions for all experiments. 0.2 μm polytetrafluoroethylene (PTFE) membrane was bought from VWR International, LLC.

2.2 Photo-oxidation experiments

Photolytic experiments for Mn^{2+} oxidation were carried out in a 150 mL quartz reactor under a 450 W Xe-arc lamp (Newport 6279NS) equipped with a water optical filter to remove infrared light. The lamp provided stable light exposure with an irradiance intensity of ~3.7 kW/m^2. The light spectrum of xenon arc lamp is shown in Fig. S1. Although the high irradiance intensity helped accelerate the reaction, the mechanism presented in this work is still representative of that under sunlight conditions. The effects of light intensity on the photolysis of nitrate and subsequent Mn^{2+} oxidation merit systematic future studies. Solutions of $MnCl_2$, $NaNO_3$, NaBr, NaCl, and SOD were exposed to the light for 6 hours.

0.1 mM $MnCl_2$ was used as the Mn source. The concentrations of dissolved Mn in natural waters can range from 10 μg/L to 10,000 μg/L (0.18 μM–0.18 mM).[21-23] Mandernack et al. examined Mn oxide mineral formation under environmentally relevant Mn concentrations of 10 μM–10 mM.[24] The Mn^{2+} concentrations used in this study might be higher than those in natural surface waters, however, these results can be useful in understanding diverse geochemical situations. In addition, 1 mM $NaNO_3$ was used in this study. According to a 2011 World Health Organization report on nitrate and nitrite in drinking water, in 1986, nitrate concentrations higher than 44 mg/L (0.71 mM) were detected in many surface water supplies.[25] Nitrate concentration can reach high levels in industrial areas or from contamination by human or animal wastes. For example, nitrate concentration can easily come up to several hundred mg/L (several mM) due to agricultural activities.[25] In addition, the ammonium in Marcellus and Fayetteville hydraulic fracturing flowback fluids can reach 420 mg/L (30 mM),[4] and it can be further converted to nitrate.

To study the effects of different reactive halogen radicals on Mn oxidation, 1 mM NaBr and 500 mM NaCl were added either separately or together into a solution. These halide concentrations

represent a highly saline aqueous environment, including seawater and other water bodies with similar concentrations. Adding 500 mM NaCl into 1 mM NaBr greatly increased ionic strength (IS) of the solution. Thus, for better comparison the same IS was maintained between different experimental conditions. Although others have substituted sodium perchlorate ($NaClO_4$) for NaCl to maintain the same IS and Na^+ concentration in a solution,[6] $NaClO_4$ was not used in this study because it could oxidize Mn^{2+} during photolysis by forming $O_2^{\bullet-}$, even without nitrate (Fig. S2). Instead, Na_2SO_4 was used to control the IS. To scavenge $O_2^{\bullet-}$, 0.5 μM SOD was utilized. We did not consider another halide ion, such as iodine, in this study because of its low concentrations in seawater (450 to 500 nM)[26] and in contaminated surface waters from the brine treatment disposal sites for hydraulic fracturing (e.g., in Pennsylvania hydraulic fracturing site, $[I^-] \leq 7.9$ μM, $[Cl^-] = 1.7$ M, $[Br^-] = 0.5$ mM)[4].

Based on the water quality criteria set by the U.S. Environmental Protection Agency (EPA), freshwater pH ranges from 6.5 to 9.[27, 28] To mimic environmentally relevant conditions, in this study, the initial pH value was adjusted to 9.0 ± 0.1 using 10 mM NaOH and the pH decreased within 6 hours as the Mn oxide solids formed. To understand the pH of the reaction systems, the pH values were continuously monitored. No pH buffer was utilized to maintain the pH, because Mn^{3+}(aq) forms strong complexation with pH buffers, such as pyrophosphate, EDTA, and citrate.[29, 30] The presence of pyrophosphate also affected the crystalline structure, morphology, and oxidation kinetics of MnO_2.[29] In addition, carbonate ions were not used to control the pH because they can react with $^{\bullet}OH$ and reactive halogen radicals to form carbonate radicals,[31, 32] which would affect Mn^{2+}(aq) oxidation processes. After 6 hr of reaction, the solution pH dropped to the range of 5–7, as shown in Fig. 2B and S2. As proved in our previous study, the pH drop was due mainly to the formation of Mn oxide solids rather than CO_2 dissolution.[17] As shown in Fig. 2A(5), during

the photolysis of 0.1 mM $MnCl_2$, 1 mM $NaNO_3$, and 0.5 μM SOD, $O_2^{\bullet-}$ was scavenged by SOD, but $^{\bullet}OH$ and dissolved CO_2 from air were still present in the solution and could form carbonate radicals. However, no Mn oxidation was observed. Thus, we expect that the concentration of CO_2 from dissolution in air in 6 hr was not sufficient to play an important role in generating carbonate radicals to induce Mn oxidation. In addition, this CO_2 dissolution process occurred under all experimental conditions and was offset when the results were compared. So the effect of carbonate radicals on Mn oxidation was not considered in this study.

2.3 Quantification of formed nanoscale Mn oxide solids

Concentrations of MnO_2 were quantified by using 0.004 % (w/v) LBB as reported before.[17, 33, 34] LBB reduced the high oxidation states of Mn(IV) and (III) in Mn oxide solids to aqueous Mn^{2+}, and then displayed a blue color (Fig. S3B). The intensity of oxidized LBB at 625 nm was proportional to the concentration of Mn oxide solids. For LBB analyses, different concentrations of $KMnO_4$ solutions were used to obtain a linear calibration curve. In these measurements, LBB analyses cannot distinguish whether the detected oxidized Mn came from solid phase of Mn oxides or aqueous oxidized Mn. Thus, 0.2 μm PTFE membrane was used to filter out the formed Mn oxide solids and leave aqueous oxidized Mn in the solution. In this way, the existence of aqueous oxidized Mn can be quantified by measuring the solutions after membrane filtration.

2.4 Phase characterization of Mn oxide solids

Photochemically-assisted synthesized solid MnO_2 products were collected by centrifugation at 10,000 rpm for 30 min. To remove impurities from the liquid supernatant, the solid products were sequentially washed, resuspended in DI water, and centrifuged five times at 5,000 rpm for 5 min. The resulting solid products were dried at room temperature for further characterization.

To identify the mineral phase of Mn oxides samples, we used high-resolution X-ray diffraction (HRXRD, Bruker D8 Advance X-ray diffractometer with Cu Kα radiation (λ = 1.5418 Å)). Because of its low saturation index (SI) of -1.20 and solubility product constant (k_{sp}) of 1.6×10^{-13},[35] $Mn(OH)_2$ (s) was not expected to form under above experimental conditions. MINEQL+ Version 4.6 was used to calculate the saturation indices for typical Mn(III)/Mn(IV) oxides based on pH ranging from pH 9 to 6. Common Mn oxide minerals, for example, birnessite (δ-MnO_2), pyrolusite (β-MnO_2), hausmannite (Mn_3O_4), and manganite (MnOOH) have SI values of 9.48–5.89, 11.54–7.95, 15.26–4.16, and 6.96–3.29, respectively, making them possible precipitates.

Mn oxidation states in the Mn oxides samples were identified by X-ray photoelectron spectroscopy (XPS, PHI 5000 VersaProbe II, UlvacPHI with monochromatic Al Kα radiation (1486.6 eV)). The C 1s peak (284.8 eV) was employed as the reference peak. To determine the ratio of Mn(II), Mn(III) and Mn(IV), the Mn $2p_{3/2}$ spin orbit was fitted with Mn(II) (640.8eV), Mn(III) (641.8 eV) and Mn(IV) (642.2 eV) by the Gauss-Lorentz fitting method. Sources for the fitting reference values of Mn(II), Mn(III), and Mn(IV) are listed in Table S1. An environmental scanning electron microscope (ESEM, ThermoFisher Quattro S) with an energy dispersive X-ray spectrometer (EDX) was used to characterize the surface morphology and material composition. Mn oxides samples were placed on a silicon wafer and visualized at a 10 mm working distance with a 10 kV accelerating voltage.

To characterize the crystalline phases and morphology of Mn oxide solids, high resolution transmission electron microscopy (HRTEM, JEOL-2100F) was used. The Mn oxide solids were well dispersed by sonication for about 15 min. Then a droplet of the suspension was placed on an ultrathin lacey carbon film coated-Cu grid (LC400-Cu-UL, Electron Microscopy Science, PA) for imaging. Lattice fringes and selective area electron diffraction images were obtained to identify

the phases of Mn oxide solids. To measure the height (thickness) of MnO_2 nanosheets, tapping mode atomic force microscopy (AFM) using a Nanoscope V multimode scanning probe microscope (SPM, Veeco Inc., NY) in air was used. To measure the hydrodynamic diameter and zeta potential of Mn oxide nanosheets in solutions, a Zetasizer Nano (Malvern Nano ZS) was used.

2.5 Alternative method to generate Br radicals

Photolysis of BrAP was used in an alternative method to generate Br radicals using a solution of 0.1 mM $MnCl_2$, 1 mM BrAP, and 0.5 μM SOD under photolysis. Mn oxide concentration and pH were measured every minute. At least duplicate tests were conducted for each condition.

3. Results and Discussion

3.1 ROS Responsible for Mn^{2+} oxidation

Fig. 1A shows the reaction pathways that generate nitrogen oxide radicals ($NO^{\bullet}$ or $NO_2^{\bullet}$), oxide radical anion ($O^{\bullet-}$), $O_2^{\bullet-}$, and $^{\bullet}OH$ during nitrate photolysis.[20] Among these products, $O_2^{\bullet-}$ and $^{\bullet}OH$ are the most common and most strongly reactive oxidants. We recently proved that the production of ROS by nitrate photolysis can lead to fast oxidation of Mn^{2+} to nanoscale Mn oxide solids by $O_2^{\bullet-}$, even without organics or microorganisms.[17] In the current study, we found that a solution containing 0.1 mM $MnCl_2$ and 1 mM $NaNO_3$ at initial pH 9 changed solution color from transparent to yellowish (Fig. S3A). Using LBB analysis, about 13.4 ± 1.0 μM of Mn oxide solids (based on Mn(IV) oxidation state) were formed within 6 hr reaction, as shown in Fig. 2A(2). With 0.5 μM of SOD, a $O_2^{\bullet-}$ scavenger, no Mn oxidation was observed (Fig. 2A(5)), confirming that $O_2^{\bullet-}$ radicals are majorly responsible for Mn oxidation, which is similar with biotic Mn oxidation by extracellular $O_2^{\bullet-}$ radicals[13-16]. We have systematically proved $^{\bullet}OH$ radicals have little contribution for Mn oxide formation in our previous study.[33] An addition of *tert*-butyl alcohol, a

scavenger of $^{\bullet}OH$ did not suppress Mn oxide formation and indeed increased the oxidation, supporting that Mn^{2+} is majorly oxidized by $O_2^{\bullet-}$ rather than $^{\bullet}OH$.[17, 33] While $^{\bullet}OH$ radicals are powerful oxidants, they have a much shorter diffusion length and half-life (nanoseconds) compared with $O_2^{\bullet-}$ (seconds).[36, 37] These limitations may influence Mn^{2+} oxidation by $^{\bullet}OH$. When the pH became lower, slower Mn oxidation was observed. Mn oxidation was preferred at higher pH,[38] and the decay of $O_2^{\bullet-}$ can be faster at lower pH values, inhibiting Mn oxidation.[39]

3.2 Faster Mn^{2+} oxidation in the presence of bromide radicals

Interestingly, in the presence of an additional 1 mM NaBr during nitrate photolysis, 62% more Mn^{2+}(aq) was oxidized within 6 hr of reaction than that without NaBr (Fig. 2A(1)). Also, the pH of a solution of 0.1 mM $MnCl_2$, 1 mM $NaNO_3$, and 1 mM NaBr decreased to ~5.0 by 6 hr reaction (Fig. 2B), faster than that without NaBr (decreased to ~ pH 6.0), due to the facilitated generation of Mn oxide solids. Fig. 2A(3) shows that Mn oxide solids formed even in a solution of 0.1 mM $MnCl_2$, 1 mM $NaNO_3$, 1 mM NaBr, and 0.5 μM SOD, indicating that new oxidant species, rather than $O_2^{\bullet-}$, were oxidizing Mn^{2+}(aq) to Mn oxide solids. We hypothesized that the additional Mn oxidation could be attributed to the Br radicals formed by the reactions between $^{\bullet}OH$ and Br^-. To test this hypothesis, Na_2SO_4 was substituted for NaBr. Mn oxidation was not detected in a solution of 0.1 mM $MnCl_2$, 1 mM $NaNO_3$, 1 mM Na_2SO_4, and 0.5 μM SOD (Fig. 2A(4)). Additionally, no Mn oxidation was observed in a solution of 0.1 mM $MnCl_2$ and 1 mM NaBr during photolysis (Fig. S4A), indicating that NaBr cannot directly oxidize Mn^{2+} during photolysis. Thus, we concluded that the additional Mn oxide solids are formed by Br radicals generated from the series of reactions between NaBr and $^{\bullet}OH$ (Fig. 1B). In the presence of Br radicals, 62% more Mn oxidation was observed than that without Br^-, suggesting that abiotic Mn oxidation by reactive radicals makes a significant contribution in nature. Halogen radicals can transform to nonradical

halogen oxidants (e.g., hypohalous acid, HOX), as shown in Equations 1 and 2 below,[5] which can then oxidize Mn^{2+} to Mn oxide solids.[40]

$$X^{\bullet} + {}^{\bullet}OH \rightarrow HOX \quad (1)$$

$$X_2^{\bullet-} + {}^{\bullet}OH \rightarrow HOX + X^- \quad (2)$$

However, such nonradical oxidants are not the major loss pathways for halogen radicals.[5] HOX can further react with $O_2^{\bullet-}$ to form $^{\bullet}OH$ and X^-,[41] and thus HOX is unlikely to be a major cause of Mn^{2+} oxidation.

In addition to Mn oxide solid phase formation, we further explored whether reactive halogen radicals can oxidize Mn^{2+} to stable aqueous species, i.e., Mn(III)–halide complexation at circumneutral pH. Aqueous samples were taken every hour from a solution containing 0.1 mM $MnCl_2$, 1 mM $NaNO_3$, 1 mM NaBr, and 0.5 μM SOD. The samples were filtered through 0.2 μm polytetrafluoroethylene (PTFE) filters three times to remove all Mn oxide solids in the solution before measuring the Mn(III)–halide concentration. This filtration is necessary because the LBB method only detects the oxidized Mn concentration but cannot distinguish whether it is in the solid or aqueous phase. In the filtered solution (Fig. S4B), no oxidized aqueous Mn species was detected via the LBB method, which confirmed the absence of aqueous Mn(III) complex in the solution. The initial pH of the solution also affected the Mn oxidation rate (Fig. S5). Compared with an initial pH of 9, a slower Mn oxidation rate was observed at an initial pH of 6.

3.3 Validation of Mn oxidation by Br radicals

To further validate the finding that Mn^{2+} can be oxidized by reactive halogen radicals, BrAP was used to directly produce $Br^{\bullet}$ by photolysis (Fig. 3),[42] rather than generating it from the reaction between halides and $^{\bullet}OH$ formed by nitrate photolysis. Because the generated $Br^{\bullet}$ can rapidly react with OH^- to form $^{\bullet}OH$, and further produce to $O_2^{\bullet-}$ via chain reactions (Fig. 3A),[6] the potentially

formed $O_2^{\bullet-}$ was scavenged by adding SOD. Fig. 3B shows the results of 4 min of photolysis of a solution containing 0.1 mM $MnCl_2$, 1 mM BrAP, and 0.5 μM SOD. About 3 μM Mn oxide solids (based on Mn(IV) oxidation state) were produced, and the solution pH dropped from 5.5 to 4.4, further proving that Mn^{2+} was indeed oxidized by reactive halogen radicals. Taken together, the above results clearly demonstrated that reactive halogen radicals can contribute significantly to the formation of Mn oxide solids from aqueous Mn^{2+}.

3.4 The different contributions of Cl and Br radicals to Mn^{2+} oxidation

While $^{\bullet}OH$ had little contribution to oxidizing Mn^{2+}(aq) to Mn oxide solids, $^{\bullet}OH$ can react with halide ions (Cl^- or Br^-) to form reactive halogen radicals that oxidize Mn^{2+}(aq). As shown in Fig. 1B, halide ions can be oxidized to monatomic radicals ($Cl^{\bullet}$ or $Br^{\bullet}$) by $^{\bullet}OH$.[43-45] In addition, diatomic radicals ($Cl_2^{\bullet-}$, $Br_2^{\bullet-}$, or $ClBr^{\bullet-}$) can be generated.[43-45] To understand the effects of different halide ions contribution and different ion concentrations on Mn oxidation, we tested Mn oxidation using a solution containing 0.1 mM $MnCl_2$, 1 mM $NaNO_3$, 1 mM NaBr, or/and 500 mM NaCl. These NaBr and NaCl concentrations were chosen as a representative condition to study a highly saline aqueous environment. The IS of the solution was greatly changed in the solution containing 0.1 mM $MnCl_2$ and 1 mM $NaNO_3$, and 500 mM of NaCl (IS ~500 mM), compared with that of a solution containing 0.1 mM $MnCl_2$ and 1 mM $NaNO_3$, and 1 mM NaBr (IS ~2 mM). As a result, Na_2SO_4 was added to maintain the same IS between different experimental conditions for better comparison. A high IS of 500 mM strongly hindered the Mn oxidation process. Only ~7 μM Mn^{2+} was oxidized by $O_2^{\bullet-}$ after 6 hr reaction during the photolysis of a solution containing 0.1 mM $MnCl_2$, 1 mM $NaNO_3$, and 166.7 mM Na_2SO_4 (IS ~500 mM) (Fig. 4A(4)), which was only a half the Mn^{2+} oxidation amount in the solution without Na_2SO_4 at a lower IS (IS ~1 mM) (Fig. 2A(2)). Because the higher IS reduced the activity coefficient and the saturation index of precursors with

respect to forming Mn oxide solids, it provided a lower thermodynamic driving force for Mn oxide nucleation and could result in a slower formation kinetics.

The contributions of Cl^- and Br^- to Mn oxidation differed due to their different concentrations in surface water and their efficacies in reactivity. Although NaBr had a 500-fold lower concentration than NaCl, at the same IS, more Mn^{2+} was oxidized by Br radicals generated from NaBr than by Cl radicals generated from NaCl, as seen in Fig. 4A (2 and 3). Most of the $BrOH^{\bullet-}$, the intermediate radical generated from the reaction between $^{\bullet}OH$ and Br^-, as shown in Fig. 1B, can further transform to other reactive halogen radicals, such as $Br^{\bullet}$ and $Br_2^{\bullet-}$,[5, 44, 46] oxidizing Mn^{2+}. On the other hand, for Cl radicals, more than 99% of $ClOH^{\bullet-}$ reverted to $^{\bullet}OH$ and Cl^- instead of forming $Cl^{\bullet}$ and $Cl_2^{\bullet-}$.[5, 47-49] Thus, Cl radicals caused less Mn^{2+} oxidation.

When 1 mM NaBr and 500 mM NaCl were dissolved together (Fig. 4A(1)), more Mn oxide formation was observed than that from adding 1 mM NaBr or 500 mM NaCl separately (Fig. 4A(2) or (3)) at the same IS. The higher oxidation of Mn^{2+} could result from the sum of Br and Cl radicals compared with single halide radicals. In addition, the promoted Mn oxide formation could result from the reaction product in the co-presence of Br^- and Cl^-. When Br^- and Cl^- co-existed, $ClBr^{\bullet-}$ can be formed at a higher rate constant than the formation rates of $Br^{\bullet}$ and $Br_2^{\bullet-}$ from a Br^- only system.[5] Thus, we postulated that the coexistence of Br^- and Cl^- in our experimental system would generate $ClBr^{\bullet-}$, which can also oxidize Mn^{2+} to Mn oxide solids faster.

3.5 Characterization of MnO_2 solids formed by $O_2^{\bullet-}$ or/and Br radicals

HRXRD was used to obtain the crystalline structure of Mn oxide formed by Br radicals, $O_2^{\bullet-}$, and Br radicals together with $O_2^{\bullet-}$, with the results shown in Fig. 5A. The 2θ XRD peaks at about 12.3°, 24.7°, and 36.7° indicated that birnessite, δ-MnO_2 (ICDD PDF-4 #00-043-1456), was formed in all three above conditions. δ-MnO_2 produced by Br radicals was quite amorphous and less

crystalline than that formed by $O_2^{\bullet-}$. δ-MnO_2 synthesized in the co-presence of Br radicals and $O_2^{\bullet-}$ presented the highest crystallinity. HRTEM images (Fig. 5B) show a thin, nanosheet morphology, with the edge rolling up due to high surface tension. In Fig. 5C, crystalline lattices with d-spacings of 0.32 nm and 0.25 nm indicated the (002) and (110)/(200) planes of δ-MnO_2, respectively. The (001) interlayer plane was observed with a 0.51 nm d-spacing, which was smaller than that calculated from XRD measurement (~0.7 nm), probably owing to the loss of interlayer water in the high vacuum environment of TEM.[50] The selected area electron diffraction (SAED) patterns in the Fig. 5B inset were also consistent with the d-spacings of the (001), (002), and (110)/(200) planes, which further confirmed the formation of δ-MnO_2. The AFM images shown in Fig. S6 were used to measure the height (thickness) of the MnO_2 nanosheets. The lateral dimension of the MnO_2 solids was about 1.5 μm and the thickness was 4–5 nm, values that confirmed its nanosheet morphology. Because a single layer of MnO_2 is ~0.7 nm thick in ambient pressure, a 4–5 nm thickness corresponds to 6–7 layers. The hydrodynamic diameters and zeta potential value of the Mn oxide solids were measured by electrophoretic mobility measurements to provide additional physicochemical information. The hydrodynamic diameter of MnO_2 solids formed *via* 6 hr photolysis of a solution containing 0.1 mM $MnCl_2$, 1 mM $NaNO_3$, and 1 mM NaBr was 2540 ± 166 nm, which reflects the average lateral dimension sizes of MnO_2 nanosheets. The formed MnO_2 nanosheets had a negative zeta potential value of -18.9 ± 0.4 mV. The ESEM image shows a rough layered morphology, and EDX results suggest a slight percentage (0.2 %) of Na^+ incorporation into the structure (Fig. S7). The XPS image in Fig. 5D suggested that formed Mn oxide solids mainly contained Mn(III) and Mn(IV), with a very small fraction of Mn(II). In general, Mn oxidation states did not show much practical difference between Mn oxide solids formed with and without NaBr. Slightly higher proportions of Mn(II) and Mn(III) were detected in δ-MnO_2

produced in the presence of NaBr, resulting in a slightly lower Mn average oxidation state (3.67) in Fig. 5F than that in the absence of NaBr (3.73) in Fig. 5E. Please note that the Mn oxide solids generation results shown in Fig. 2A were calculated by the LBB method, which assumed that the Mn oxide solids consisted of only Mn(IV). Because the average oxidation state of Mn was lower than 4 in the XPS results, the actual concentrations of Mn oxide solids could be higher than the values in Fig. 2A.

3.6 Effects of $O_2^{\bullet-}$ or/and reactive halogen radicals on Mn^{2+} oxidation and subsequent Mn oxide nanosheet formation

To investigate the singular contributions of reactive halogen radicals (Cl and Br radicals) to Mn oxidation without $O_2^{\bullet-}$, SOD was added to scavenge $O_2^{\bullet-}$ in the solution. As shown in Fig. 4A(6), without any halides, no Mn oxidation was observed during the photolysis of a solution containing 0.1 mM $MnCl_2$, 1 mM $NaNO_3$, 166.7 mM Na_2SO_4, and 0.5 μM SOD, because neither reactive halogen radicals nor $O_2^{\bullet-}$ were present to oxidize Mn^{2+}. Substituting 1 mM NaBr and 500 mM NaCl for the 166.7 mM Na_2SO_4 caused the generation of reactive halogen radicals and Mn oxide solids formation (Fig. 4A(5)). Fig. 4B displays the Mn^{2+} oxidation amounts after 6 hr reaction under different conditions at low or high IS: $O_2^{\bullet-}$, Br and/or Cl radicals, and $O_2^{\bullet-}$ with Br and/or Cl radicals. At the same IS (the dashed box in Fig. 4B), the contribution of $O_2^{\bullet-}$, Br radicals, and Cl radicals to Mn oxide solids generation can be fairly compared. More Mn oxide nanosheets were formed during nitrate photolysis in the presence of additional halide ions. As seen in Fig. S8, for all experiments at about 500 mM IS, the solution pH changed with time, but all showed the same pH trend, decreasing from an initial pH 9.0 to pH 7.0–6.0 after 6 hr of photolysis. A slightly faster pH drop was observed with a larger amount of Mn oxide nanosheet formation.

In the coexistence of Cl and Br radicals, the HRXRD results in Fig. 6A(1) and (3) confirmed that Mn oxide had a higher crystallinity than that produced by Br radicals, as shown in Fig. 6A(2) and (4), respectively. This finding suggested that higher IS promoted the crystallization of Mn oxide, although slower kinetics for Mn^{2+} formation by Cl radicals together with Br radicals was observed than for Br radicals alone (navy blue vs. orange and black vs. blue in Fig. 4B). Based on XPS analysis, the average Mn oxidation states of Mn oxide produced by $O_2^{\bullet-}$ and/or Br radicals was 3.68−3.73 (Fig. 5D–F) under low IS conditions (i.e., less than 2 mM), while they decreased to 3.57−3.63 (Fig. 6B) under high IS conditions (~500 mM) because of larger Mn(III) and smaller Mn(IV) portions. The insignificantly lower Mn oxidation states may result from charge compensation for more Na^+ incorporation into the structure of Mn oxide nanosheets (3.4% of Na^+, Fig. 6D) at high IS compared with that at low IS (0.2% of Na^+, Fig. S7). The ESEM image in Fig. 6C showed that Mn oxide samples presented rumpled and wrinkled surface morphology. Zhang et al. (2018) reported that intercalated Na^+ tended to shift and coordinate with two unsaturated O from the MnO_6 layer via strong electrostatic interactions rather than staying in between two MnO_6 layers to balance the interactions, resulting in unbalanced supporting interstitial distances between MnO_6 layers and causing a rough surface.[51]

4. Conclusions and environmental implications

Here we show the hitherto unexplored oxidation of Mn^{2+} by reactive halogen radicals. Compared to the abiotic oxidation rate of Mn^{2+} without Br radicals, in the presence of Br radicals, the abiotic oxidation rate of Mn^{2+} to Mn oxide nanosheets was greatly facilitated, exhibiting a 62% increase within 6 hr. In the natural environment, NaBr had a much lower concentration than NaCl, however, at the same experimental IS, more Mn^{2+} was oxidized by Br radicals generated from 1 mM NaBr than by Cl radicals generated from 500 mM NaCl. δ-MnO_2 nanosheets were formed by reactive

halogen species, and increasing the IS caused more highly crystalline Mn oxides to form. Although the pH, the concentrations of Mn^{2+}, nitrate, and halides, and the intensity of light illumination obviously vary in different water bodies, this study provides a good starting point for understanding how halogen radicals are generated and affect Mn^{2+} oxidation processes. This work highlights the importance of underappreciated reactive halogen radicals in inorganic redox reactions in aqueous environmental systems. In nature, reactive halogen radicals can be produced *via* oxidation of halides by $^{\bullet}OH$, $SO_4^{\bullet-}$, or triplet state dissolved organic matter ($^3DOM^*$).[5] The natural contribution of reactive halogen radicals to Mn^{2+} oxidation and MnO_2 formation merit future systematic experiments. The redox reaction mechanism between reactive halogen radicals and $Mn^{2+}(aq)$ can be applicable to other redox-sensitive transition metal ions, such as Fe^{2+}, As^{3+}, and Cr^{3+}. Furthermore, the results are also critically valuable to understanding aerosol reactions involving halides in the atmosphere. Halide ions are preferentially present at air-water interfaces rather than in bulk solution,[52] where surface halide ions can actively react with $^{\bullet}OH$ to generate halogen radicals.[53] In the atmosphere, this behavior can amplify the effects of reactive halogen species on the oxidation of redox active metals, forming nanoscale mineral aerosols that can act as cloud condensation nuclei and affect the albedo. Moreover, compared with bulk MnO_2 particles that do not have any nanoscale planes or structures, nanoscale MnO_2 shows an improved catalytic performance for electrochemical oxygen reduction.[54] This study suggests a novel, environmentally-friendly, and facile pathway for the synthesis of MnO_2 nanosheets.

Author contributions

Z. G., C. S., and Y.-S. J. conducted the experiments. Z. G. and Y.-S. J. designed the experimental setup and procedures and wrote the manuscript. All authors discussed the results and collectively revised the manuscript.

Conflicts of Interest

The authors declare that they have no known competing financial interests or personal relationships that could have appeared to influence the work reported in this paper.

Acknowledgments

This work is supported by National Science Foundation's Environmental Chemical Sciences program (CHE-1905077). The authors would like to acknowledge the Institute of Materials Science & Engineering (IMSE) of Washington University in St. Louis for the use of XPS, ESEM, and TEM, Professor Kimberly Parker for providing suggestions, and Professor James C. Ballard for carefully reviewing the manuscript.

References

1. N. Voutchkov, Overview of seawater concentrate disposal alternatives, *Desalination*, 2011, **273**, 205-219.
2. C. Zhang, Y. Shi, L. Shi, H. Li, R. Li, S. Hong, S. Zhuo, T. Zhang and P. Wang, Designing a next generation solar crystallizer for real seawater brine treatment with zero liquid discharge, *Nat. Commun.*, 2021, **12**, 1-10.
3. K. B. Gregory, R. D. Vidic and D. A. Dzombak, Water management challenges associated with the production of shale gas by hydraulic fracturing, *Elements*, 2011, **7**, 181-186.
4. J. S. Harkness, G. S. Dwyer, N. R. Warner, K. M. Parker, W. A. Mitch and A. Vengosh, Iodide, bromide, and ammonium in hydraulic fracturing and oil and gas wastewaters: environmental implications, *Environ. Sci. Technol.*, 2015, **49**, 1955-1963.
5. K. Zhang and K. M. Parker, Halogen radical oxidants in natural and engineered aquatic systems, *Environ. Sci. Technol.*, 2018, **52**, 9579-9594.
6. K. M. Parker and W. A. Mitch, Halogen radicals contribute to photooxidation in coastal and estuarine waters, *Proc. Natl. Acad. Sci. U. S. A.*, 2016, **113**, 5868-5873.
7. K. M. Parker, E. S. Reichwaldt, A. Ghadouani and W. A. Mitch, Halogen radicals promote the photodegradation of microcystins in estuarine systems, *Environ. Sci. Technol.*, 2016, **50**, 8505-8513.
8. S. Cheng, X. Zhang, X. Yang, C. Shang, W. Song, J. Fang and Y. Pan, The multiple role of bromide ion in PPCPs degradation under UV/chlorine treatment, *Environ. Sci. Technol.*, 2018, **52**, 1806-1816.
9. C. R. Stephens, P. B. Shepson, A. Steffen, J. W. Bottenheim, J. Liao, L. G. Huey, E. Apel, A. Weinheimer, S. R. Hall and C. Cantrell, The relative importance of chlorine and bromine radicals in the oxidation of atmospheric mercury at Barrow, Alaska, *J. Geophys. Res. Atmos.*, 2012, **117**.
10. C. R. Myers and K. H. Nealson, Bacterial manganese reduction and growth with manganese oxide as the sole electron acceptor, *Science*, 1988, **240**, 1319-1321.
11. B. M. Tebo, J. R. Bargar, B. G. Clement, G. J. Dick, K. J. Murray, D. Parker, R. Verity and S. M. Webb, Biogenic manganese oxides: properties and mechanisms of formation, *Annu. Rev. Earth Planet. Sci.*, 2004, **32**, 287-328.
12. C. N. Butterfield, A. V. Soldatova, S.-W. Lee, T. G. Spiro and B. M. Tebo, Mn(II, III) oxidation and MnO_2 mineralization by an expressed bacterial multicopper oxidase, *Proc. Natl. Acad. Sci. U. S. A.*, 2013, **110**, 11731-11735.
13. D. Learman, B. Voelker, A. Vazquez-Rodriguez and C. Hansel, Formation of manganese oxides by bacterially generated superoxide, *Nat. Geosci.*, 2011, **4**, 95-98.
14. C. M. Hansel, C. A. Zeiner, C. M. Santelli and S. M. Webb, Mn(II) oxidation by an ascomycete fungus is linked to superoxide production during asexual reproduction, *Proc. Natl. Acad. Sci. U. S. A.*, 2012, **109**, 12621-12625.
15. D. Learman, S. Wankel, S. Webb, N. Martinez, A. Madden and C. Hansel, Coupled biotic–

abiotic Mn(II) oxidation pathway mediates the formation and structural evolution of biogenic Mn oxides, *Geochim. Cosmochim. Acta*, 2011, **75**, 6048-6063.

16. J. M. Diaz, C. M. Hansel, B. M. Voelker, C. M. Mendes, P. F. Andeer and T. Zhang, Widespread production of extracellular superoxide by heterotrophic bacteria, *Science*, 2013, 1237331.

17. H. Jung, T. S. Chadha, D. Kim, P. Biswas and Y.-S. Jun, Photochemically assisted fast abiotic oxidation of manganese and formation of δ-MnO_2 nanosheets in nitrate solution, *Chem. Commun.*, 2017, **53**, 4445-4448.

18. G. S. Laurence and A. T. Thornton, Kinetics of oxidation of transition-metal ions by halogen radical anions. Part III. The oxidation of manganese(II) by dibromide and dichloride ions generated by flash photolysis, *J. Chem. Soc., Dalton Trans.*, 1973, 1637-1644.

19. G. Davies, Some aspects of the chemistry of manganese(III) in aqueous solution, *Coord. Chem. Rev.*, 1969, **4**, 199-224.

20. J. Mack and J. R. Bolton, Photochemistry of nitrite and nitrate in aqueous solution: a review, *J. Photochem. Photobiol. A: Chem.*, 1999, **128**, 1-13.

21. WHO, *Concise international chemical assessment document 12, Manganese and its compounds*, World Health Organization, 1999.

22. WHO, *Concise international chemical assessment document 63, Manganese and its Compounds: Environmental Aspects*, World Health Organization, 2004.

23. M. Williams, G. D. Todd, N. Roney, J. Crawford, C. Coles, P. R. McClure, J. D. Garey, K. Zaccaria and M. Citra, Toxicological profile for manganese, 2013.

24. K. W. Mandernack, J. Post and B. M. Tebo, Manganese mineral formation by bacterial spores of the marine *Bacillus*, strain SG-1: Evidence for the direct oxidation of Mn(II) to Mn(IV), *Geochim. Cosmochim. Acta*, 1995, **59**, 4393-4408.

25. WHO, *Nitrate and nitrite in drinking-water*, World Health Organization 2011.

26. R. Chance, A. R. Baker, L. Carpenter and T. D. Jickells, The distribution of iodide at the sea surface, *Env. Sci. Process. Impact.*, 2014, **16**, 1841-1859.

27. EPA, *Quality criteria for water*, 1986.

28. EPA, pH, https://www.epa.gov/caddis-vol2/caddis-volume-2-sources-stressors-responses-ph, (accessed January 18, 2021).

29. H. Jung, T. S. Chadha, Y. Min, P. Biswas and Y.-S. Jun, Photochemically-assisted synthesis of birnessite nanosheets and their structural alteration in the presence of pyrophosphate, *ACS Sustainable Chem. Eng.*, 2017, **5**, 10624-10632.

30. J. K. Klewicki and J. J. Morgan, Kinetic behavior of Mn(III) complexes of pyrophosphate, EDTA, and citrate, *Environ. Sci. Technol.*, 1998, **32**, 2916-2922.

31. R. E. Huie, C. L. Clifton and P. Neta, Electron transfer reaction rates and equilibria of the carbonate and sulfate radical anions, *International Journal of Radiation Applications and Instrumentation. Part C. Radiation Physics and Chemistry*, 1991, **38**, 477-481.

32. S. Yan, Y. Liu, L. Lian, R. Li, J. Ma, H. Zhou and W. Song, Photochemical formation of carbonate radical and its reaction with dissolved organic matters, *Water Res.*, 2019, **161**, 288-296.

33. Z. Gao, D. Zhang and Y.-S. Jun, Does *tert*-butyl alcohol really terminate the oxidative activity of •OH in inorganic redox chemistry?, *Environ. Sci. Technol.*, 2021, **55**, 10442-10450.

34. M. R. Jones, G. W. Luther III, A. Mucci and B. M. Tebo, Concentrations of reactive Mn(III)-L and MnO_2 in estuarine and marine waters determined using spectrophotometry and the leuco base, leucoberbelin blue, *Talanta*, 2019, **200**, 91-99.

35. R. K. Fox, D. F. Swinehart and A. Garrett, The equilibria of manganese hydroxide, $Mn(OH)_2$, in solutions of hydrochloric acid and sodium hydroxide, *J. Am. Chem. Soc.*, 1941, **63**, 1779-1782.

36. M. Levy, P. P. Chowdhury and P. Nagpal, Quantum dot therapeutics: a new class of radical therapies, *J. Biol. Eng.*, 2019, **13**, 48.

37. K. Krumova and G. Cosa, Overview of reactive oxygen species, 2016.

38. Z. Gao, J. Liu, C. Skurie, Y. Zhu and Y.-S. Jun, Photochemical reactions of dissolved organic matter and bromide ions facilitate abiotic formation of manganese oxide solids, *Water Res.*, 2022, 118831.

39. J. Ma, H. Zhou, S. Yan and W. Song, Kinetics studies and mechanistic considerations on the reactions of superoxide radical ions with dissolved organic matter, *Water Res.*, 2019, **149**, 56-64.

40. S. Allard, L. Fouche, J. Dick, A. Heitz and U. von Gunten, Oxidation of manganese(II) during chlorination: role of bromide, *Environ. Sci. Technol.*, 2013, **47**, 8716-8723.

41. E. M. Rodríguez and U. von Gunten, Generation of hydroxyl radical during chlorination of hydroxyphenols and natural organic matter extracts, *Water Res.*, 2020, **177**, 115691.

42. W. McGimpsey and J. Scaiano, Photochemistry of α-chloro-and α-bromoacetophenone. Determination of extinction coefficients for halogen–benzene complexes, *Can. J. Chem.*, 1988, **66**, 1474-1478.

43. P. F. De Violet, Polyhalide radical anions as intermediates in chemistry, *Reviews of Chemical Intermediates*, 1981, **4**, 121-169.

44. D. Zehavi and J. Rabani, Oxidation of aqueous bromide ions by hydroxyl radicals. Pulse radiolytic investigation, *J. Phys. Chem.*, 1972, **76**, 312-319.

45. X.-Y. Yu and J. R. Barker, Hydrogen peroxide photolysis in acidic aqueous solutions containing chloride ions. I. Chemical mechanism, *The Journal of Physical Chemistry A*, 2003, **107**, 1313-1324.

46. G. Merenyi and J. Lind, Reaction mechanism of hydrogen abstraction by the bromine atom in water, *J. Am. Chem. Soc.*, 1994, **116**, 7872-7876.

47. G. Jayson, B. Parsons and A. J. Swallow, Some simple, highly reactive, inorganic chlorine derivatives in aqueous solution. Their formation using pulses of radiation and their role in the mechanism of the Fricke dosimeter, *J. Chem. Soc., Faraday Trans. 1 F*, 1973, **69**, 1597-

1607.

48. A. Grigor'ev, I. Makarov and A. Pikaev, Formation of Cl_2^- in the bulk of solution during radiolysis of concentrated aqueous solutions of chlorides, *Khimiya Vysokikh Ehnergij*, 1987, **21**, 123-126.

49. U. K. Kläning and T. Wolff, Laser flash photolysis of HClO, ClO^- , HBrO, and BrO^- in aqueous solution. reactions of Cl- and Br-atoms, *Ber. Bunsenge. Phys. Chem.*, 1985, **89**, 243-245.

50. J. Zhu, Q. Li, W. Bi, L. Bai, X. Zhang, J. Zhou and Y. Xie, Ultra-rapid microwave-assisted synthesis of layered ultrathin birnessite $K_{0.17}MnO_2$ nanosheets for efficient energy storage, *J. Mater. Chem. A*, 2013, **1**, 8154-8159.

51. T. Zhang, L. Liu, W. Tan, S. L. Suib, G. Qiu and F. Liu, Photochemical formation and transformation of birnessite: Effects of cations on micromorphology and crystal structure, *Environ. Sci. Technol.*, 2018, **52**, 6864-6871.

52. P. Jungwirth and D. J. Tobias, Ions at the air/water interface, *J. Phys. Chem. B*, 2002, **106**, 6361-6373.

53. E. Knipping, M. Lakin, K. Foster, P. Jungwirth, D. Tobias, R. Gerber, D. Dabdub and B. Finlayson-Pitts, Experiments and simulations of ion-enhanced interfacial chemistry on aqueous NaCl aerosols, *Science*, 2000, **288**, 301-306.

54. F. Cheng, Y. Su, J. Liang, Z. Tao and J. Chen, MnO_2-based nanostructures as catalysts for electrochemical oxygen reduction in alkaline media, *Chem. Mater.*, 2010, **22**, 898-905.

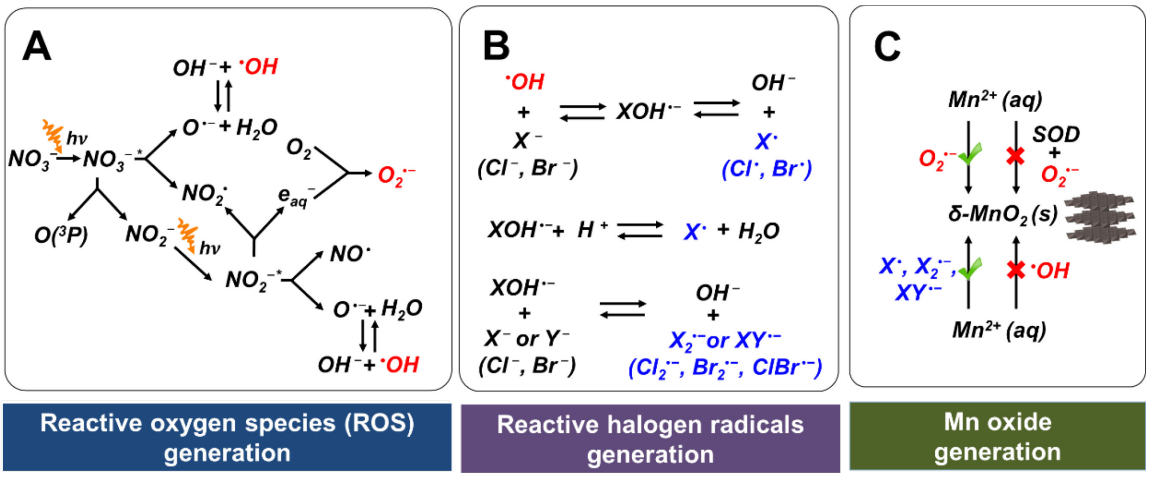

Figure 1. Schematics of the generation pathways of ROS and reactive halogen radicals, and Mn^{2+} oxidation pathways. (A) Chain reactions in the generation of $O_2^{\bullet-}$ and $^{\bullet}OH$ during nitrate photolysis. (B) Chain reactions in the generation of reactive halogen radicals. (C) Mn^{2+}(aq) oxidation by $O_2^{\bullet-}$ and reactive halogen radicals.

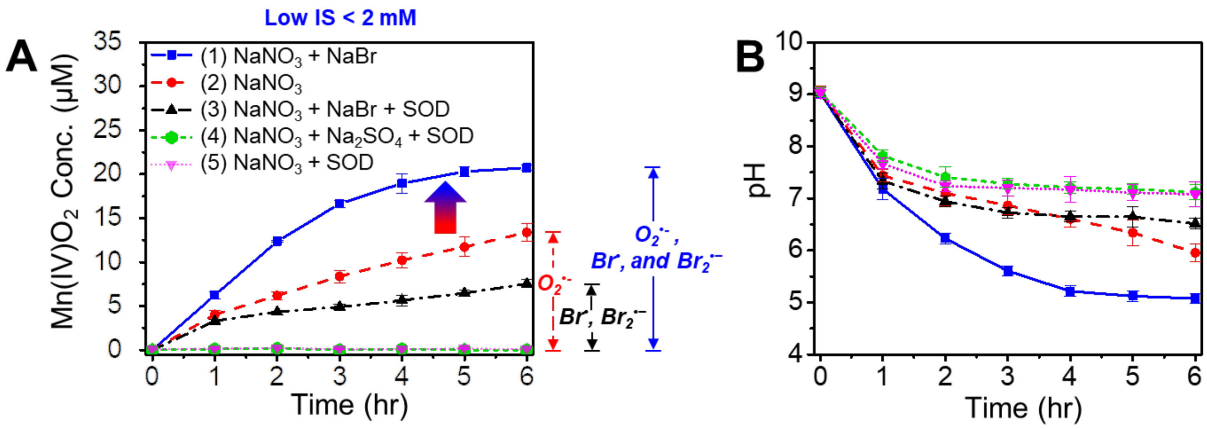

Figure 2. Oxidation of Mn^{2+}(aq) to Mn oxide solids by $O_2^{\bullet-}$ or/and Br radicals**.** (A) Oxidized Mn concentrations and (B) pH values during 6 hr of photolysis of solutions containing (1) 0.1 mM $MnCl_2$, 1 mM $NaNO_3$, and 1 mM NaBr; (2) 0.1 mM $MnCl_2$ and 1 mM $NaNO_3$; (3) 0.1 mM $MnCl_2$, 1 mM $NaNO_3$, 1 mM NaBr, and 0.5 μM SOD; (4) 0.1 mM $MnCl_2$, 1 mM $NaNO_3$, 1 mM Na_2SO_4, and 0.5 μM SOD; and (5) 0.1 mM $MnCl_2$, 1 mM $NaNO_3$, and 0.5 μM SOD. Error bars represent standard errors of the data obtained from duplicate experiments.

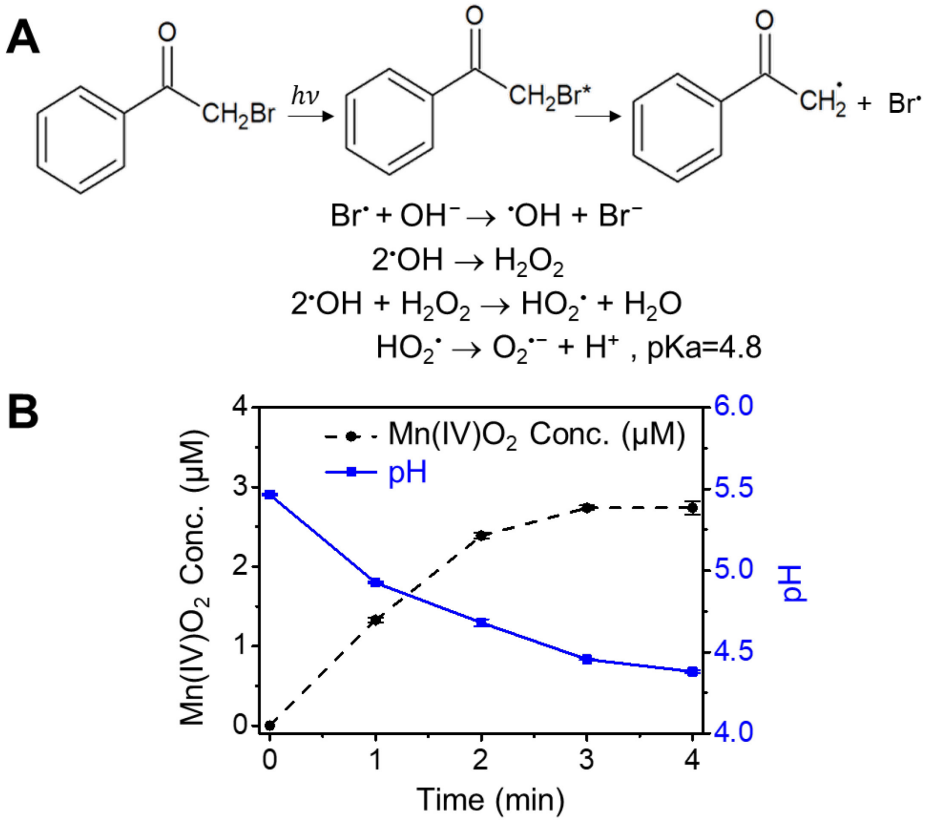

Figure 3. Mn oxidation by Br radicals generated from photolysis of bromoacetophenone (BrAP). (A) Photolysis of BrAP can produce $Br^{\bullet}$, which can react with OH^- to form $^{\bullet}OH$. $O_2^{\bullet-}$ is potentially formed in the sequential reactions. (B) Oxidized Mn concentration and pH value during photolysis of solution containing 0.1 mM $MnCl_2$, 1 mM BrAP, and 0.5 μM SOD. Error bars represent standard errors of the data obtained from duplicate experiments.

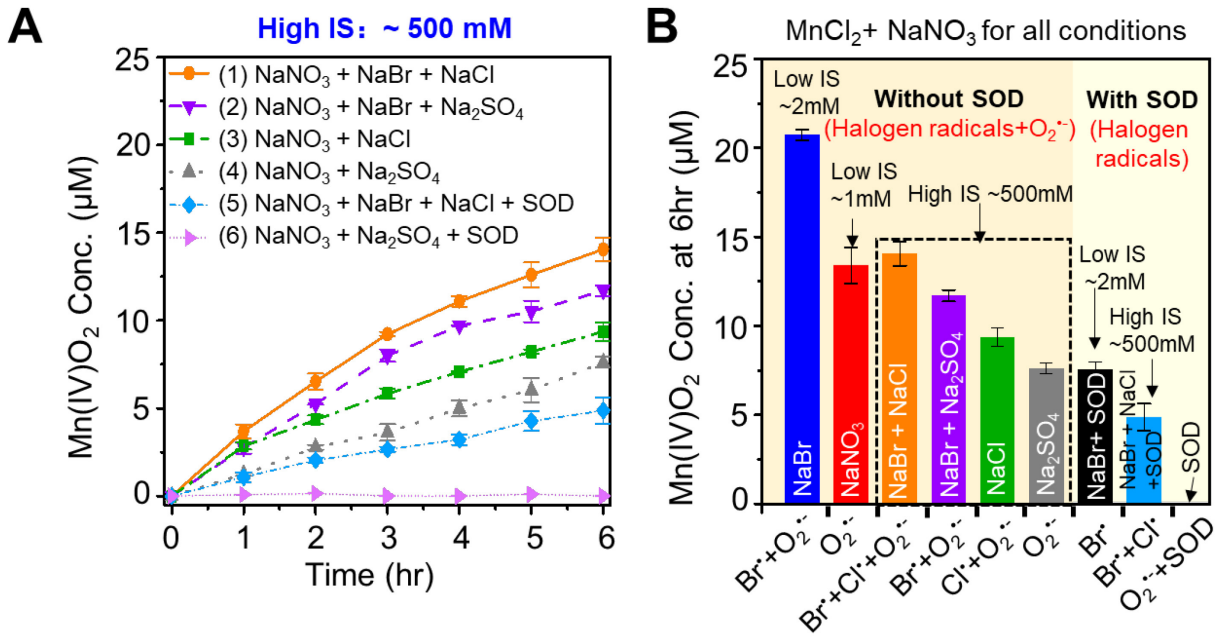

Figure 4. Comparison of the kinetics of Mn^{2+}(aq) oxidation by $O_2^{\bullet-}$ or/and reactive halogen radicals (Br or/and Cl radicals). (A) Mn oxide generation over 6 hr of photolysis reaction of 0.1 mM $MnCl_2$, 1 mM $NaNO_3$ with different halide compositions at the same IS (~500 mM) without/with SOD. (1) 0.1 mM $MnCl_2$, 1 mM $NaNO_3$, 1 mM NaBr, and 500 mM NaCl; (2) 0.1 mM $MnCl_2$, 1 mM $NaNO_3$, 1 mM NaBr, and 166.7 mM Na_2SO_4; (3) 0.1 mM $MnCl_2$, 1 mM $NaNO_3$, and 500 mM NaCl; (4) 0.1 mM $MnCl_2$, 1 mM $NaNO_3$, and 166.7 mM Na_2SO_4; (5) 0.1 mM $MnCl_2$, 1 mM $NaNO_3$, 1 mM NaBr, 500 mM NaCl, and 0.5 μM SOD; and (6) 0.1 mM $MnCl_2$, 1 mM $NaNO_3$, 166.7 mM Na_2SO_4, and 0.5 μM SOD. (B) Summary of Mn^{2+} oxidation amounts of all conditions after 6 hr reaction. In the horizontal axis title, $Br^{\bullet}$ stands for Br radicals ($Br^{\bullet}$ and $Br_2^{\bullet-}$), $Cl^{\bullet}$ stands for Cl radicals ($Cl^{\bullet}$ and $Cl_2^{\bullet-}$), and $Br^{\bullet}$ + $Cl^{\bullet}$ stands for all Cl and Br radicals ($Cl^{\bullet}$, $Br^{\bullet}$, $Cl_2^{\bullet-}$, $Br_2^{\bullet-}$, and $ClBr^{\bullet-}$).

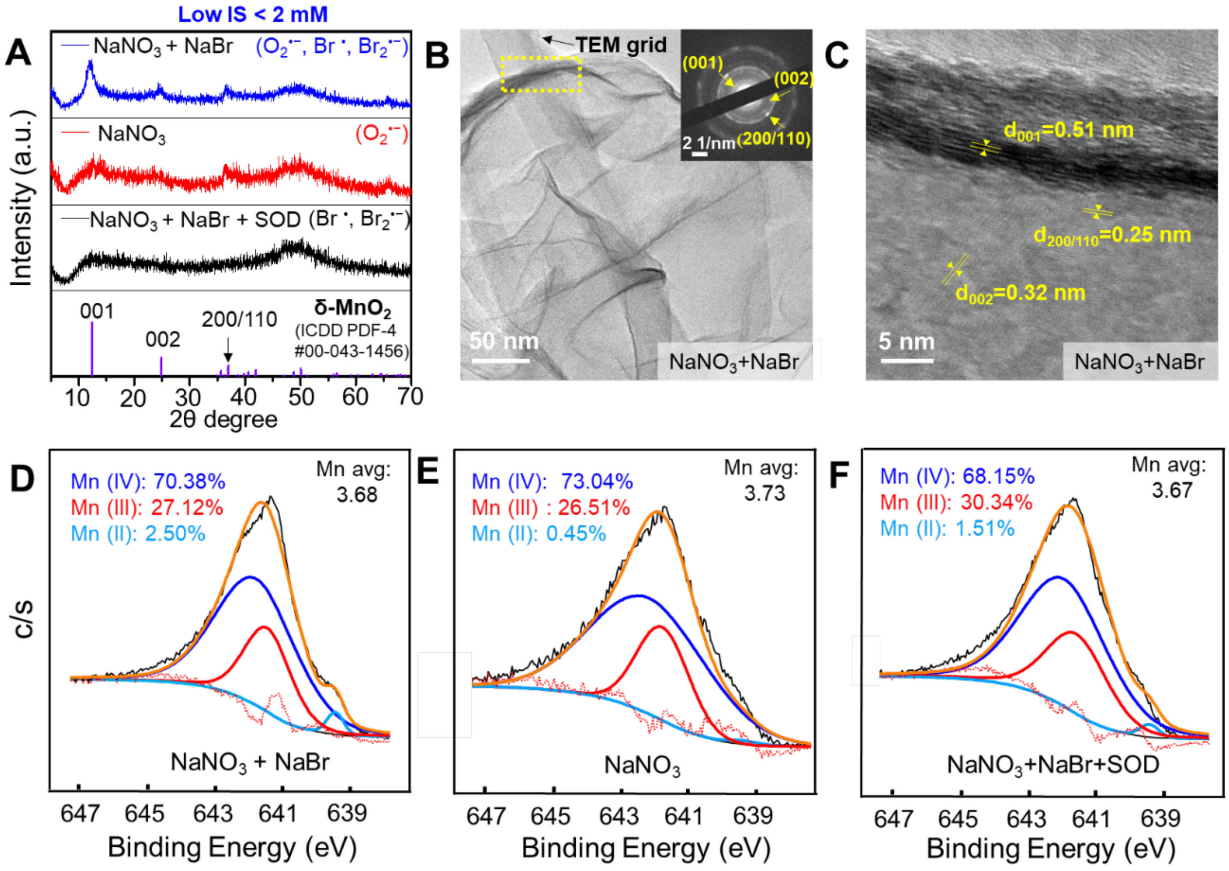

Figure 5. MnO_2 nanosheets formed by Br radicals. (A) δ-MnO_2 formation measured by HRXRD under the conditions of 0.1 mM $MnCl_2$, 1 mM $NaNO_3$, and 1 mM NaBr (blue); 0.1 mM $MnCl_2$ and 1 mM $NaNO_3$ (red); and 0.1 mM $MnCl_2$, 1 mM $NaNO_3$, 1 mM NaBr, and 0.5 μM SOD (black) after 6 hr of reaction. (B and C) HRTEM images of the synthesized Mn oxide nanosheets under the condition of 0.1 mM $MnCl_2$, 1 mM $NaNO_3$, and 1 mM NaBr. The SAED patterns in (B) confirmed the formation of δ-MnO_2. (D-F) Average Mn oxidation states of the Mn $2p_{3/2}$ spectrum, calculated via Gaussian-Lorentzian fitting. Mn oxide solids were generated under the conditions listed in (A). At least duplicate tests were conducted for each condition. At least five different spots in the TEM grids were measured.

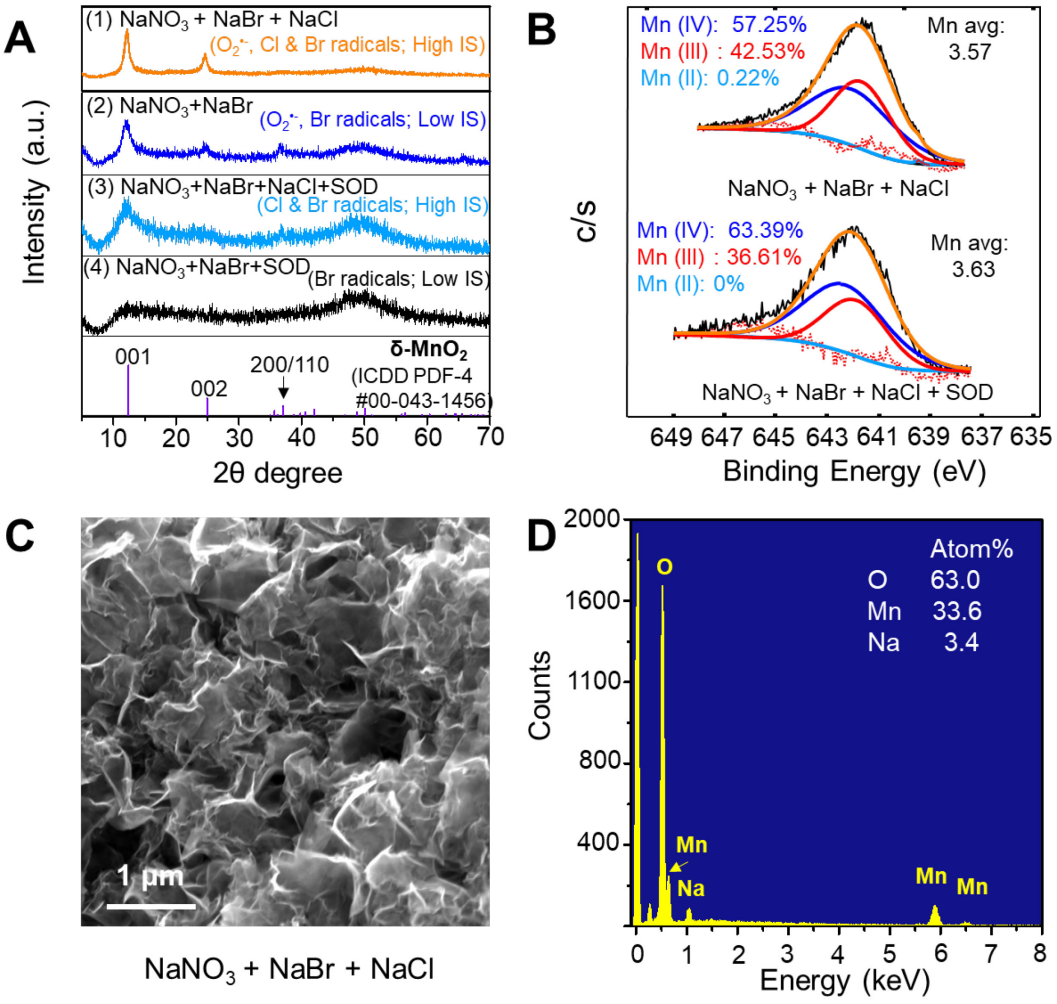

Figure 6. Comparison of $O_2^{\bullet-}$ or/and reactive halogen radicals on the characteristics of newly formed Mn oxide solids. (A) Comparison of HRXRD spectra of Mn oxide solids formed under the conditions of (1) 0.1 mM $MnCl_2$, 1 mM $NaNO_3$, 1 mM NaBr, and 500 mM NaCl; (2) 0.1 mM $MnCl_2$, 1 mM $NaNO_3$, and 1 mM NaBr; (3) 0.1 mM $MnCl_2$, 1 mM $NaNO_3$, 1 mM NaBr, 500 mM NaCl, and 0.5 μM SOD; and (4) 0.1 mM $MnCl_2$, 1 mM $NaNO_3$, 1 mM NaBr and 0.5 μM SOD. (B) Average Mn oxidation state of Mn $2p_{3/2}$ spectrum calculated via Gaussian-Lorentzian fitting. Mn oxide solids were formed under the conditions of (1) and (3). (C and D) Images showing surface morphology and elemental composition of Mn oxide formed under the condition of (1). At least duplicate tests were conducted for each condition. At least five different spots were measured for SEM imaging.